ELSEVIER

Polymer 43 (2002) 1641–1648

polymer

www.elsevier.com/locate/polymer

Spatially resolved electron diffraction and the determination of orientational order parameters in thermotropic liquid crystalline polymer

Jennifer E. Taylor[a], Angel Romo-Uribe[b], Matthew R. Libera[a,*]

[a]*Department of Chemical, Biochemical and Materials Engineering, Stevens Institute of Technology, Castle Point on Hudson, Hoboken, NJ 07030, USA*
[b]*Ticona (Celanese AG), 86 Morris Avenue, Summit, NJ 07901, USA*

Received 3 April 2001; received in revised form 18 October 2001; accepted 19 October 2001

Abstract

A low-dose, high-resolution, electron-diffraction technique has been used to calculate *local* orientational order parameters from thermotropic liquid crystal polymer (TLCP) fibers. Diffracted intensities are extracted from digital electron diffraction patterns for the orientational order parameter calculation, in a manner similar to that used with X-ray diffraction data. The resolution of local orientation is made possible by electron diffraction as opposed to other methods because of the ability to sample regions as small as 100 nm in diameter. Working within the critical radiative dose for structural damage constrains the ultimate spatial resolution. The signal-to-noise ratio (SNR) of the diffraction data collected at high spatial resolution is low due to the small volume sampled. This work demonstrates the dependence of the orientational order parameter on signal-to-noise effects and the convergence of the incoming electron beam.

Keywords: Orientational order parameter; Hydroxybenzoic acid/hydroxynaphthoic acid; Transmission electron microscopy

1. Introduction

The determination of molecular orientation has been instrumental in defining the structure–processing–properties relationship in a variety of polymeric materials where molecular anisotropy is present. Such materials range from cellulose gels [1,2] and common thermoplastics like polystyrene [3], polyethylene [4], nylon 6 [5], polypropylene [6], and polyethylene terephthalate [7] to liquid crystalline polymers (LCP), both thermotropic [8] (TLCP) and lyotropic [9] (LLCP). Recent development of in situ microscopic probes has enabled the correlation of molecular orientation with bulk properties like viscosity and stress [10–12]. Knowledge of the morphology of oriented materials is an essential condition for the development of any theoretical interpretation of deformation mechanics [13] and, ultimately, the most finely engineered mechanical properties.

A number of analytical techniques have been developed for quantitative measurement of molecular orientation. Birefringence [14], sonic velocity propagation [15], and spectroscopic techniques such as infrared dichroism [16] and nuclear magnetic resonance (NMR) [17,18] have also been applied. A clear disadvantage of these techniques is that they are limited by the ability to provide high spatial resolution compared to other characterization methods. Some improvement in this respect is found by using wide-angle X-ray scattering (WAXS) [8,19,20]. Even higher spatial resolution has been achieved by using electron diffraction techniques such as scanning transmission electron microscopy (STEM) [21–23].

WAXS is favored over spectroscopic methods for the determination of the degree of preferred orientation in TLCPs. Diffraction is little affected by changes such as localized rotation of polar pendant groups, which might occur independently of chain orientation and lead to confusion when measuring orientation from birefringence or infrared dichroism [8,24,25]. Furthermore, WAXS can give the complete orientation distribution [8]. The quantification of orientation parameters is based on even-ordered Legendre polynomials. These polynomials can describe an orientation distribution function from an anisotropic system having a preferred orientation around an axis of symmetry [8]. Molecular orientation in liquid crystalline materials is defined in terms of a molecular director expressed as a unit vector $\mathbf{n}$ ($+\mathbf{n}$ and $-\mathbf{n}$ are physically equivalent). The director is parallel to the mean orientation of the molecules in the neighborhood of a given point [26]. Orientational order parameters, $\langle P_2 \rangle_D$, are a measure of the distribution of molecular orientations around the director. Values range

* Corresponding author. Fax: +1-201-216-8306.
E-mail address: mlibera@stevens-tech.edu (M.R. Libera).

0032-3861/02/$ - see front matter
PII: S0032-3861(01)00717-0

between 0 and 1, where the former corresponds to an isotropic structure and the latter represents total alignment along the director.

The conventional electron diffraction technique presented in this paper enables quantification of molecular alignment at length scales of the order of 100–200 nm, which is approximately an order of magnitude improvement in spatial resolution over other techniques. However, it should be noted that an advantageous feature of some of the X-ray and neutron scattering methods over electron diffraction is that they can be performed in situ to provide real time measurements during rheological studies [11,12,27,28]. A clear disadvantage of those techniques is that the smallest area from which a diffraction pattern is collected is larger than characteristic fine scale structural features believed to be present in intrinsically ordered materials such as TLCP. For example, crystalline regions have been reported in high molecular weight hydroxybenzoic acid (HBA) hydroxynaphthoic acid (HNA) copolyester to be approximately 12 nm thick, 60 nm wide, and 250 nm in length [29]. Furthermore, structural gradients of molecular orientations, termed as 'skin-core effect' [30], have been observed in fibers and injection-molded parts. The high intensity of synchrotron X-ray radiation enables resolution of 1 μm by microfocus and capillary techniques [31]. Although this is a considerable improvement over traditional X-ray and neutron scattering techniques, nanoscale structures are still averaged over a micron scale area.

The calculation of orientational order parameters used here is based on the method derived for X-ray diffraction by Mitchell and Windle [8,32–34]. The distribution of molecular orientations in the diffraction patterns collected from LCP fibers can be modeled in terms of even-ordered Legendre polynomials, because the distribution of orientation has uniaxial and inversion symmetry. In this work, only the second order Legendre polynomial, also termed the Herman's orientation function, is used to quantify molecular alignment. The order parameter of the intensity measured experimentally is a convolution of the order parameter associated with the distribution of domains or single molecules and the orientation parameter from a perfectly oriented region or molecule. Since the orientation parameters are representations in reciprocal space, the total intensity becomes a product, and the orientational order parameter for the distribution, $\langle P_2\rangle_D$, can be written as

$$\langle P_2\rangle_D = \frac{\langle P_2\rangle_I}{\langle P_2\rangle_I^m} \tag{1}$$

where $\langle P_2\rangle_I$ is the orientation parameter of the experimentally measured intensity distribution and $\langle P_2\rangle_I^m$ is the orientation parameter of a perfectly aligned region. The normalized amplitude for the total intensity is written in terms of the azimuthal intensities, $I(\alpha)$, collected from the diffraction patterns

$$\langle P_2\rangle_I = \frac{\int_0^{\pi/2} I(\alpha)P_2(\cos\alpha)\sin\alpha\,\mathrm{d}\alpha}{\int_0^{\pi/2} I(\alpha)\sin\alpha\,\mathrm{d}\alpha} \tag{2}$$

where α is the azimuthal angle. In the case of X-ray diffraction studies, where the signal-to-noise ratio (SNR) is high, the azimuthal intensity distribution for a perfectly oriented sample is approximated by a delta function with a single point of intensity at $\alpha = \pi/2$. $\langle P_2\rangle_I^m$ becomes equal to $-1/2$. Background-subtracted azimuthal intensities, $I(\alpha)$, from digital diffraction patterns and the approximated value of $\langle P_2\rangle_I^m$ are applied to Eqs. (1) and (2) to obtain the orientational order parameters representative of the molecular distribution.

The detectable signal of diffracted peaks taken at high spatial resolution is necessarily small, because of constraints imposed by the incident radiative dose. At one extreme, the *minimum* dose required to get a meaningful signal above noise is inversely proportional to the area sampled [35]. At the other extreme, the *maximum* dose is limited by changes in the specimen induced by the incident ionizing radiation. Following the convention set by Spontak et al. [36], a critical dose can be defined as the electron dose that causes the intensity specific Bragg diffracted peak to fall to 10% of its initial value. The radiative dose is defined as

$$D = \frac{jt}{s} \tag{3}$$

where j is the electron current, t is the time of exposure, and s is the sampled area. There is a limited range of acceptable doses that can be used to collect diffraction patterns at high spatial resolution before the quality of data is compromised by radiation damage effects.

The convergence of the electron probe necessary to form smaller sampling areas also influences the calculated orientational order parameters. The Bragg reflections broaden with radii proportional to the convergence angle [37]. This is due to the range of incident angles that the partially converged incoming electron waves possess upon interaction with the specimen. On the other hand, parallel incident radiation (no convergence angle) gives sharp peaks, because the incident beam interacts with the specimen from only one angle. Since a diffracted spot is broadened by this convergence effect, the angular distribution of the azimuthal intensity profile will be larger than when using perfectly parallel radiation. However, convergence can be easily corrected since the size of the sampled area remains constant for a given experiment. The convergence angle is determined using the following equation [38]

$$2\gamma = 2\theta_B\frac{a}{b} \tag{4}$$

where γ is half of the total convergence angle, $2\theta_B$ is the

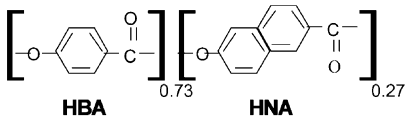

Fig. 1. Chemical structure of 73 mol% 1,4-hydroxybenzoic acid and 27 mol% 2,6-hydroxynaphthoic acid.

known Bragg angle of a particular reflection, a is the diameter of that particular Bragg reflection, and b is the distance from the (000) reflection to the (hkl) reflection associated with $2\theta_B$. There is an intrinsic breadth of the diffracted spots due to the point-spread function (PSF) associated with an electron detector even without any convergence of the incident beam [39]. However, this is negligible for the calculation of orientational order parameters as will be shown later.

This paper describes an electron diffraction technique that enables orientational order parameters to be calculated from areas as small as 100 nm in diameter. The improved spatial resolution gives a more precise depiction of structural variations by reducing the sampled area over which the structure is averaged. The technique is applied to wholly aromatic as-spun and heat-treated Vectran®[1] fibers that were spun from the thermotropic copolyester based on HBA and HNA.

This investigation will show that orientational order parameters determined by electron diffraction are comparable to those obtained by X-ray scattering measurements after proper account for lower SNR and the contribution from the convergence angle is considered. However, even without correcting for these effects, a 15% increase in the orientation parameters is observed for heat-treated fibers compared to as-spun fibers [8]. The fact that heat-treated fibers display a higher degree of molecular orientation is consistent with previous findings that annealing leads to straighter and more tightly packed molecules [40]. This clearly indicates that the spatially resolved electron diffraction technique is able to distinguish a distinct degree of molecular orientation at spatial resolutions on the order of 100 nm.

2. Experimental

2.1. Materials

Commercial Vectran® liquid crystal polymer fiber, typically 18 μm in diameter (Celanese Americas), was supplied both as-spun and heat-treated. These fibers were spun from the thermotropic Vectra®[2] A950 copolyester (Ticona—formerly Hoechst Celanese) composed of approximately 73 mol% 1,4-hydroxybenzoic acid and 27 mol% 2,6-hydroxynaphthoic acid (Fig. 1). The as-spun fiber was heat-treated by ramping the temperature to 270 °C and then holding there for 4–20 h. Fibers were mounted in epoxy and sliced longitudinally by microtomy at room temperature. Each section, with a typical thickness of 80–100 nm, was placed on a copper TEM grid covered by a holey carbon support film. The holey carbon film substrate was necessarily used for structural support of the fiber section.

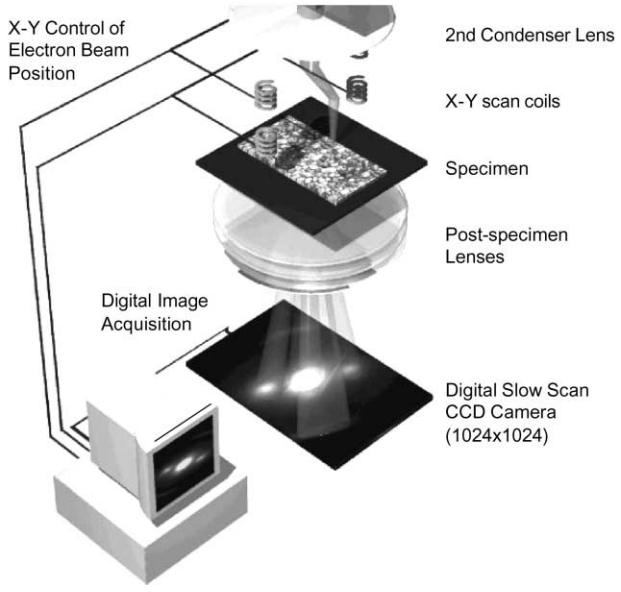

Fig. 2. Experimental setup showing digital control of electron beam and acquisition of digital data using a CCD camera.

Signal-to-noise and convergence-angle measurements were performed using a MoO_3 TEM specimen. This specimen was chosen because acicular single-crystal needles form with their long edge oriented along the [001] direction [41]. These crystals provide predictable single-crystal diffraction patterns that are invariant with respect to the spatial resolution of the incident electron beam.

2.2. Measurement of molecular orientation by transmission electron microscopy

A Philips CM20 transmission electron microscope (TEM) with a field emission gun (FEG) electron source was used for electron diffraction experiments. A 30 μm diameter condenser aperture was used to reduce the effects of electron-beam convergence on the breadth of relevant Bragg reflections. Diffraction patterns of as-spun and heat-treated HBA/HNA fibers were collected from areas as small as ~100 nm in diameter. The data were collected in digital form using a Gatan 794 Retractable Slow Scan CCD camera. The set up of the apparatus is shown in Fig. 2. A detailed description of the experimental set up can be found elsewhere [42].

Gatan's Digital Micrograph version 3.3 image processing software was used to extract azimuthal intensities. Azimuthal traces were found from a scan of 360° mapped to 360 pixels at $\mathbf{q} = 0.20\,\text{A}^{-1}$ which corresponds to the (110) equatorial peak. Each point of the azimuthal trace

[1] Vectran is a trademark of Celanese.
[2] Vectra is a trademark of Ticona.

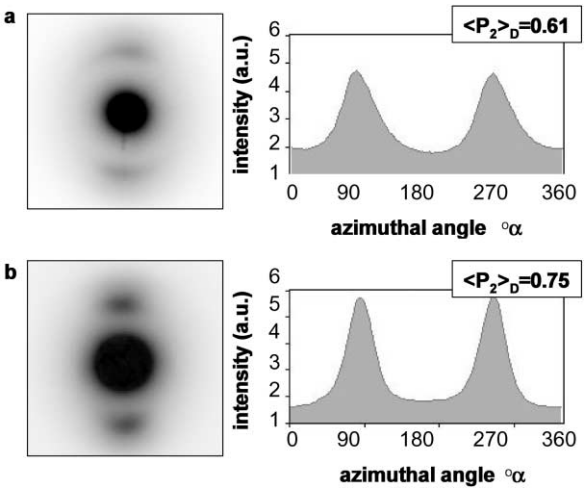

Fig. 3. Electron diffraction patterns and normalized azimuthal intensity traces for as-spun and heat-treated fibers. The corresponding orientational order parameters are indicated in each plot.

was an integrated value of intensity over ±2 pixels perpendicular to the tangent. This ensured that the entire (110) reflection was taken into account [25]. Azimuthal intensity traces were generated by extracting values between 0 and 360° where the centers of the diffracted equatorial maxima are located at 90 and 270°. A background value from each pattern was subtracted to eliminate incoherent intensity [34,43,44] arising from inelastic scattering as well as scattered intensity from the carbon support film. The lowest intensity value (at 0°) was designated as the background value [8,34]. Since the amorphous diffraction halos from the carbon support film are located at different values of **q**, the amorphous carbon support film contributed no significant intensity. Orientational order parameters were calculated by substituting the background-subtracted intensity values into Eq. (2) for each azimuthal angle.

2.3. Radiative dose measurements

The measurement of the critical radiative dose was performed by calibrating the microscope's photographic exposure meter with the electron current. The electron current was measured using a Faraday Cup and a picoammeter. After this calibration, incident electron beam current could be conveniently determined by reading the microscope's exposure meter under conditions where the electron beam passed unobstructed through a perforation in the specimen. The diameter of the irradiated area was determined by real-space measurements using the slow scan camera. For incident spot sizes above approximately 10 nm in diameter, the intensity distribution of the incident electron beam could be approximated as a top-hat function. Diffraction patterns from each specimen were recorded at varying dose levels, and an azimuthal intensity profile was extracted from each diffraction pattern. The maximum of the diffracted peak height was measured from each azimuthal intensity profile for all electron doses and plotted to find the critical dose. The critical dose was defined to be the dose where the peak height decayed by 10% from its initial value.

2.4. Signal-to-noise and convergence measurements

Several exposures of diffraction patterns were collected at the same location on a thin MoO_3 crystal to determine the effects of SNR and beam convergence on the orientation parameter. For the SNR studies, the dimensions of the sampled area remained constant throughout the series while the exposure time was varied. SNR was defined as the diffracted peak height in the azimuthal intensity profile divided by the standard deviation of the noise (after background subtraction). To observe the effect of increasing the convergence angle of the electron beam, the exposure time was kept constant while the sampled area was varied from 750 to 100 nm. The influence of radiative dose on the MoO_3 was not considered here since it is not radiation sensitive under the present experimental conditions.

2.5. Measurement of molecular orientation by X-ray scattering

WAXS patterns of the same HBA/HNA fiber were obtained in symmetrical transmission mode. The patterns were electronically recorded using the general diffraction detector system (GADDS) and the Hi-Star® area detector manufactured by Brüker AXS. The *d*-spacing was calibrated using Corundum (A1203) powder, and the incident X-ray beam was collimated to 500 μm diameter. The GADDS system was mounted on a Rigaku rotating anode X-ray generator SU-200 with a copper anode. A plane-crystal incident-beam monochromator was fitted to the diffractometer; a Union Carbide oriented graphite monochromator was used (grade ZYA, with mosaic spread of 0.4° ± 0.1°). The residual K_β component was removed by the angle-selective effect of the collimation system. Prior to the extraction of

Table 1
Orientational order parameters characteristic of as-spun and heat-treated HBA/HNA fiber

	Calculated from ED patterns (±0.02)	Corrected value (±0.02)	Calculated from X-ray scattering (±0.02)
As-spun HBA/HNA fiber	0.45–0.68	0.55–0.83	0.83
Heat-treated HBA/HNA fiber	0.67–0.75	0.86–0.96	0.90

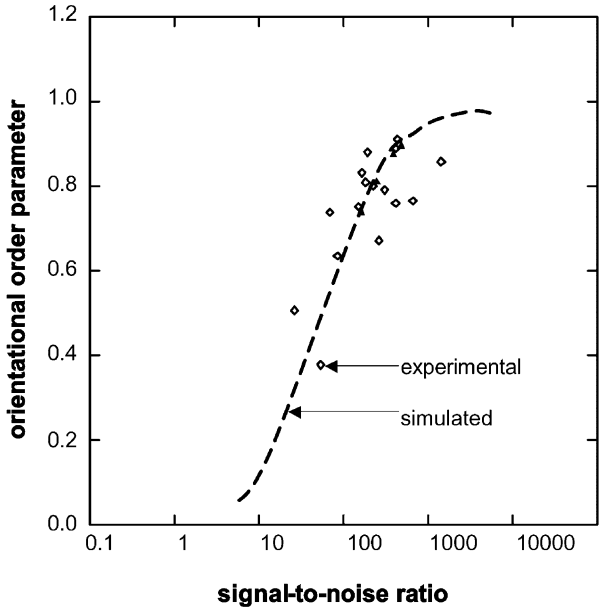

Fig. 4. Effect of SNR on calculated orientational order parameter of MoO_3 single crystal. Orientation parameters have been normalized to 1 by dividing throughout by $-1/2$.

intensities, the diffraction patterns were spatially corrected following the manufacture's procedure. The degree of orientation was quantified from the integrated intensities, $I(\alpha)$, of the main equatorial maxima as a function of the azimuthal angle α [25].

3. Results

The azimuthal intensity and the corresponding diffraction patterns from the as-spun and heat-treated fibers are shown in Fig. 3 where the azimuthal intensity has been normalized using the integrated intensity under the peak. The as-spun material has a lower peak intensity and a broader distribution of intensities than the heat-treated fiber. This difference is reflected in the corresponding orientational order parameters. Table 1 shows a comparison of measured order parameters in the as-spun and heat-treated fibers along with the values obtained from X-ray studies of the same fibers. The order parameters obtained for both as-spun and heat-treated fibers were lower than those obtained by wide-angle X-ray measurement. Nevertheless, a range of values from 0.45 to 0.68 is observed within the as-spun fibers indicating that this technique is indeed able to detect a variation in the degree of orientation within the fibers. The orientation parameters determined from heat-treated fibers are higher and have a narrow range of values compared to the as-spun fibers. As stated earlier, the deviations from the expected results based on X-ray data are mainly attributed to two systematic effects: SNR and convergence angle.

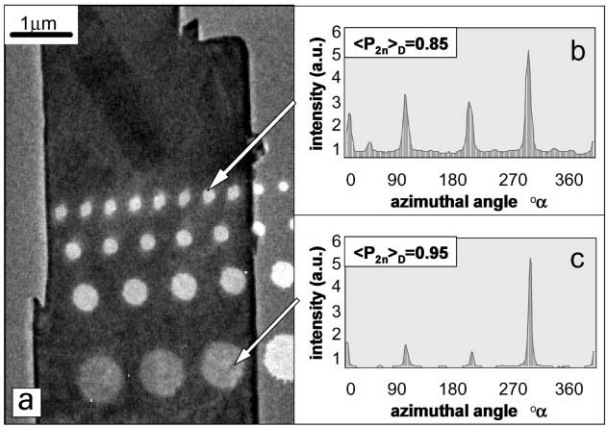

Fig. 5. (a) Bright-field TEM image of a MoO_3 crystal with images of electron probes ranging from ~100 to 750 nm in diameter. Azimuthal intensity traces and calculated orientational order parameters of electron diffraction patterns from an area (b) 100 nm and (c) 750 nm in diameter are shown.

Orientational order parameters obtained with the spatially resolved electron diffraction technique are smaller than expected, compared to the parameters obtained using X-ray diffraction. This is mainly due to the lower SNR characteristic of enhanced spatial resolution. Simply put, the amount of signal obtainable from a radiation-sensitive material decreases as the sampling volume decreases. A MoO_3 single crystal was used to observe the decrease in orientational order parameter for a perfectly oriented sample, $\langle P_2\rangle_I^m$, as a function of SNR. Fig. 4 shows a plot of orientation parameter as a function of SNR where the open symbols correspond to experimental data points. The $\langle P_2\rangle_I^m$ values were each normalized to 1 by dividing by $-1/2$. The solid line is the result of a simulation discussed in Section 4.

The convergence of the electron beam necessary to form sub-micron sampling areas also affects the measured orientational order parameter. As shown in Fig. 5b and c, the azimuthal intensity profiles become broader when the sampled areas shown in Fig. 5a are reduced from 750 to 100 nm in diameter. Fig. 6 shows the decreasing dependence of the orientational order parameter as a function of convergence angle. Overall, the orientational order parameter decreases by approximately 10% when the sampled area is reduced from 750 to 100 nm. This spatial range corresponds to an increase in convergence angle from 0.70 to 1.83 mrad. These experimental results suggest that the convergence effect would become more significant if the electron beam was further focused towards the limiting case of convergence angle on the order of 10 mrad, which is the case of a fully converged electron beam.

The critical dose values characteristic of as-spun and heat-treated 73/27 HBA/HNA fibers were determined using diffraction patterns collected from the same area after varying the exposure time. Fig. 7 shows diffraction patterns collected from a heat-treated fiber (a) unexposed to radiation before acquisition and (b) exposed to a dose of 30 000 C/m^2 prior to acquisition. Both samples were exposed to 40 C/m^2 during collection of the diffraction patterns. Fig. 7b shows almost no indication of the equatorial peaks shown in the

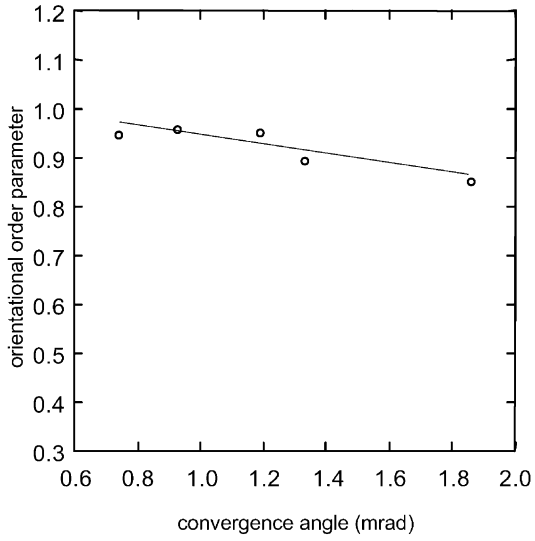

Fig. 6. The orientational order parameter decreases with increasing convergence angle. The continuous line corresponds to a linear fit to the experimental data.

diffraction pattern of Fig. 7a corresponding to a loss in crystallinity. The critical dose is measured by defining the dose of the onset of radiation damage as shown in Fig. 8. It can be seen that the onset of radiation damage is preceded by several orders of dose where there is negligible change in the peak height. When the critical dose is defined in terms of change in diffracted peak height, the critical dose value for as-spun fibers is $\sim$125 C/m^2 compared to the heat-treated value of $\sim$850 C/m^2. These values are slightly higher than those determined by Spontak et al. [36,45] for wholly aromatic TLCP which is attributed to the fact that the materials studied here have lower molecular weight [46]. The values

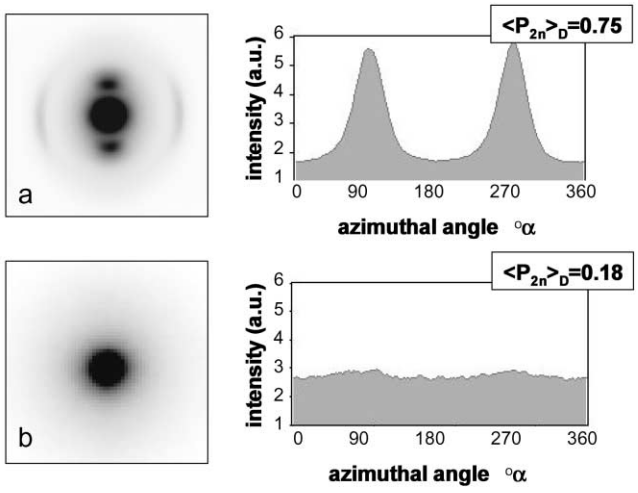

Fig. 7. (a) Electron diffraction pattern and corresponding azimuthal intensity traces of heat-treated HBA/HNA fiber. No previous irradiation of sample. (b) Diffraction pattern and corresponding azimuthal intensity traces of heat-treated fiber after exposure to a dose of 30 000 C/m^2.

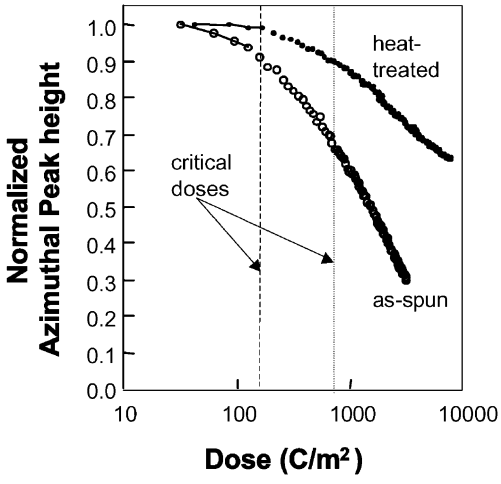

Fig. 8. Critical dose measurements of as-spun and heat-treated HBA/HNA fiber.

reported here would be significantly higher if the less conservative criterion for critical dose, 1/*e* of the initial value was used.

4. Discussion

This investigation has shown that the spatially resolved electron diffraction technique is able to discern different levels of molecular orientation within a highly oriented material such as a fiber of TLCP. The orientational order parameters found using electron diffraction should be comparable to those determined by X-ray diffraction, however. The fact that the values determined from electron diffraction are lower than those obtained by X-ray is attributed to systematic effects associated with achieving high spatial resolution by forming a sub-micron electron probe. The lower values of orientational order parameters are attributed to lower signal-to-noise values and to the convergence of the electron beam. However, the fact that the orientation parameters of well-oriented fibers (heat-treated) are higher than the less-oriented fibers (as-spun) confirms that the electron-diffraction technique can distinguish different degrees of molecular alignment.

Low SNR is unavoidable at high spatial resolution, because the signal is inversely related to the sampled volume [35]. Less volume is sampled when the measurement is pushed to higher spatial resolution. This effect is entirely independent of the type of radiation used. To assess how the orientation parameter decreases with decreasing SNR, azimuthal intensities were collected from a single crystal of MoO_3 for a broad range of incident doses. However, it should be pointed out that the signal necessary to get an orientation parameter of 1 would require oversaturation of the CCD camera by the transmitted spot. By simulating diffraction patterns from a perfect crystal, this problem was circumvented. Fig. 9 shows the procedure

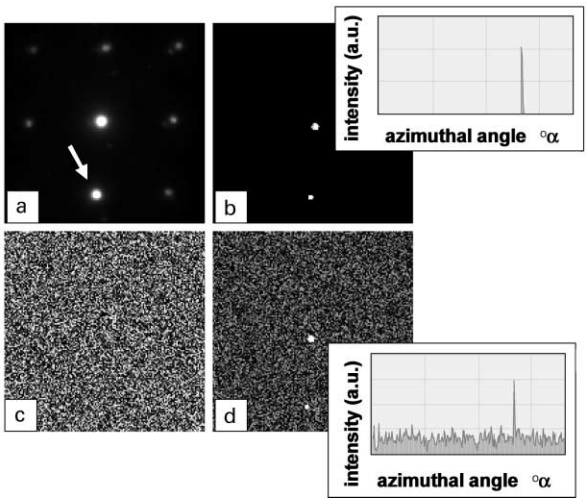

Fig. 9. Simulation of azimuthal intensity with varying SNR. (a) An electron diffraction pattern of MoO_3 single crystal where a (100) reflection is indicated. (b) All pixels except the (100) and (00$\bar{0}$) peaks are set to zero as shown in the top right inset. The maximum intensity of (100) diffracted peak intensity is set to 1. (c) Random noise image with pixel values between 0 and 1. Pixels corresponding to any reflection are set to 0. (d) The addition of (b) and (c). The lower right inset is the resulting azimuthal trace corresponding to the sum of the reflection shown in (a) and the noise shown in (c).

followed to obtain diffraction patterns where the amount of generated noise and the height of the diffracted peak is systematically altered. Fig. 9a shows the original diffraction pattern from a MoO_3 single crystal that was used to create the simulated diffraction patterns. Fig. 9b shows a diffraction pattern where all the pixels in Fig. 9a except the forward-scattered (000) peak and the Bragg diffracted peak of interest were set to zero. The azimuthal intensity that results from the pattern in Fig. 9b is approximately a delta function at 268°. Fig. 9c shows random noise with intensity values from 0 to 1, where the pixels corresponding to the peak of interest are set to zero. By multiplying the pixels in this image by any number, the standard deviation of the noise is manipulated. Fig. 9d shows the sum of Fig. 9b and c and the corresponding azimuthal intensity scan. Repeating this procedure for a range of different backgrounds (Fig. 9c), a decreasing exponential dependence of the orientational order parameter on SNR is observed as shown in Fig. 4. The solid line in Fig. 4 represents the values of $\langle P_2 \rangle_I^m$ found by the simulation. Since the intrinsic width of the diffracted peak is included in the patterns used for the simulation and the results show that the orientation parameter goes to 1 at high values of SNR, the effect of the point spread function is considered negligible.

The orientational order parameters determined by electron diffraction becomes comparable to the values determined by X-ray after corrections are made for SNR and convergence effects. Typical SNR values are ~600 and convergence angles for as-spun and heat-treated samples are 1.33 and 1.83 mrad, respectively. The value of $\langle P_2 \rangle_I^m$ for this SNR is 0.88 (Fig. 4). $\langle P_2 \rangle_I^m$ must be further reduced by 0.06 and 0.10 to account for the convergence angles used during the sampling of the different fibers. Thus, the final values of $\langle P_2 \rangle_I^m$ that are substituted into Eq. (1) are 0.82 and 0.78 for as-spun and heat-treated samples, respectively. Table 1 shows the corrected orientational order parameter values for as-spun and heat-treated fibers. A broad range of orientation parameters is observed compared to X-ray results, because variations within the larger irradiated areas of the X-ray technique are averaged over much smaller distances using the electron diffraction technique. The fact that a range of values is observed at higher spatial resolution indicates that these fibers contain morphological elements of order 100 nm in size or smaller with their own characteristic orientation. This point is being addressed in ongoing research.

5. Conclusion

The measurement of molecular orientational order parameters using electron diffraction is an effective means of quantifying sub-micron orientation in materials with spatially dependent microstructure such as LCP fibers. Application of electron diffraction to as-spun and heat-treated HBA/HNA fibers shows that the critical dose limits are sufficiently high to obtain orientation parameters from specimen dimensions as small as 100 nm in diameter. A dependence on SNR is evident when orientational order parameters are found at high spatial resolution. After correction of this factor, orientational order parameters that are calculated from electron diffraction patterns are similar to those found by X-ray diffraction. Increasing the convergence angle by focusing the electron beam to obtain high spatial resolution causes an additional effect on the orientational order parameter due to broadening of the diffracted spots. After properly accounting for these effects, the structural variations within as-spun and heat-treated thermotropic LCP fibers are observed at length scales as small as 100 nm in a manner consistent with X-ray scattering data collected at significantly lower spatial resolution.

Acknowledgements

The authors would like to thank Linda Sawyer of Ticona (Celanese AG) for providing the LCP fibers used in this research and for much valuable insight. This research was supported by the Army Research Office through grant numbers DAAG55-97-1-0137 and DAAG55-98-1-0150.

References

[1] Hermans PH, Hermans JJ, Vermaas D, Weidinger A. J Polym Sci 1948;3(1):1–9.
[2] Andresen EM, Mitchell GR. Polymer 1998;39:7127–9.
[3] Hermans JJ, Hermans PH, Vermaas D, Weidinger A. Recl Trav Chim 1946;65:427–33.

[4] Katayama K, Amano T, Nakamura K. Polymer 1977;18:913–24.
[5] Ishibashi T, Ishii T. J Polym Sci 1976;20:335–42.
[6] Ishizuka O, Koyama K. Polymer 1977;18(9):913–8.
[7] Thompson AB. Fiber structure. London: Applied Science, 1963.
[8] Mitchell GR, Windle AH. Orientation in liquid crystal polymers. In: Bassett DC, editor. Developments in crystalline polymers, 2nd ed. Essex: Elsevier, 1988. Chapter 2.
[9] Picken SJ. Macromolecules 1990;23:464–70.
[10] Ward IM. Structure and properties of oriented polymers. New York: Wiley, 1975.
[11] Janeschitz-Kriegl H. Polymer melt rheology and flow birefringence. Berlin: Springer, 1983.
[12] Romo-Uribe A. Proc R Soc Lond A 2001;457:207–29.
[13] Romo-Uribe A, Windle AH. Proc R Soc Lond A 1999;455:1175–201.
[14] Ward IM. Structure and properties of oriented polymers. New York: Wiley, 1975.
[15] Moseley WW. J Appl Polym Sci 1960;3:266.
[16] Read BE. In: Ward IE, editor. Structure and properties of oriented polymers. New York: Wiley, 1975. Chapter 4.
[17] Liao MY, Rutledge GC. Macromolecules 1997;30:7546–53.
[18] McArdle CB. Side chain liquid crystal polymers. New York: Chapman & Hall, 1989.
[19] Windle AH. Measurement of molecular orientation and structure in non-crystalline polymers by wide-angle X-ray scattering. London: Applied Science, 1982.
[20] Alexander LE. X-ray diffraction methods in polymer science. New York: Wiley, 1969.
[21] Low A, Vesely D, Allan P, Bevis M. J Mater Sci 1978;13:711–21.
[22] Sherman ES, Adams WW, Thomas EL. J Mater Sci 1981;16:1–9.
[23] Roche EJ, Stein RS, Thomas EL. J Polym Sci, Polym Phys Ed 1980;18:1145–58.
[24] Leadbetter AJ. Structural studies of nematic, smectic A, and smectic C phases. In: Luckhurst GR, Gray GW, editors. The molecular physics of liquid crystals. London: Academic Press, 1979. p. 285–319.
[25] Haase W, Fan Z-X, Muller HJ. J Chem Phys 1988;89:3317–22.
[26] De Gennes PG. The physics of liquid crystals. Oxford: Clarendon Press, 1974.
[27] Romo-Uribe A, Lemmon TJ, Windle AH. J Rheol 1997;41(5):1117–45.
[28] Romo-Uribe A, Mather PT, Chaffee KP, Han CD. Mater Res Soc Symp Proc 1997;461:63–8.
[29] Donald AM, Windle AH. J Mater Sci Lett 1985;4:58–60.
[30] Sawyer LC, Jaffe M. J Mater Sci 1986;21:1897–913.
[31] Fuller W. J Appl Crystallogr 1999;32:1127–33.
[32] Pick M, Lovell R, Windle AH. Polymer 1980;21:1018–25.
[33] Lovell R, Mitchell GR. Acta Crystallogr 1981;A30:135–7.
[34] Mitchell GR, Windle AH. Polymer 1983;24:1513–20.
[35] Howie A. Rev Phys Appl 1980;15:291.
[36] Spontak RJ, Windle AH. J Mater Sci 1990;25:2727–36.
[37] Spence JC, Zuo JM. Electron microdiffraction. New York: Plenum Press, 1992.
[38] Williams D, Carter B. Transmission electron microscopy. New York: Plenum Press, 1996.
[39] Zhou JM. Ultramicroscopy 1996;66:21–33.
[40] Ward IM. Polymer 1997;38(21):5355–61.
[41] Thomas G, Goringe MJ. Transmission electron microscopy of materials. New York: Wiley, 1979.
[42] Taylor J, Libera M, Greeley M. Mater Res Soc Symp Proc 1999;559:128–34.
[43] Hsiung CM, Cakmak M. Antec 1991:1063–70.
[44] Al-Ammar KH, Mitchell GR. Polymer 1992;33(1):11–21.
[45] Spontak RJ, Windle AH. Polymer 1990;31:1395–400.
[46] Spontak RJ, Windle AH. J Polym Sci B 1992;30:61–9.